NUMERICAL SIMULATION OF COMBUSTION CHARACTERISTICS AND NO_X EMISSION IN A 330 MW POWER PLANT BOILER WITH SELF-SUSTAINING INTERNAL COMBUSTION BURNER

Hong TANG[1], Jing YANG[1], Ivan TOMANOVIĆ[2], Guojia YAO[1,*], Xiaoju HAN[1]

[*1] School of Automation Engineering, Northeast Electric Power University, Jilin, 132012, China

[2]Department of Thermal Engineering and Energy, "VINČA" Institute of Nuclear Sciences-National Institute of the Republic of Serbia, University of Belgrade, Mike Petrovica Alasa 12-14, 11351 Belgrade, Serbia

[*] Corresponding author; E-mail: yaoguojia@neepu.edu.cn

Nitrogen oxides (NO_X) emitted from coal-fired power plants are one of the primary sources of NO_X in the atmosphere. More stringent requierements on NO_X emissions are implemented in laws focusing on the environmental protection. The self-sustaining internal combustion (SSIC) burner can stably preheat the pulverized coal and produce reducing atmosphere, effectively reducing NO_X emissions, but the SSIC burners are still not widely used in industrial boilers. The SSIC burner is being used on a 330 MW tangentially-fired boiler to reduce NO_X emissions from the boiler and improve stabilized combustion performance. The effect of the SSIC burner on the flow, combustion and NO_X emission characteristics of the boiler are investigated by numerically simulating the boiler before and after retrofit at different loads (100% and 70%). The findings indicate that the initial NO_X emission at the outlet is reduced by 24.77% and 27.18%, respectively, when the boiler with SSIC burner is operated at 100% and 70% loads. The combustion stability is improved and the pulverized coal burnout rate is increased by 2.22% and 2.46%, respectively. The NO_X emissions of the boiler with the SSIC burner is reduced to 91.73 mg/Nm^3 at 70% load. The SSIC burner employed in the 330 MW tangentially fired boiler has been shown to achieve effective NO_X reduction and can be adapted to the changing demands of the boiler load. This study offers beneficial guidance for the practical implementation of SSIC burners on industrial power station boilers.

Key words*: combustion; boiler; preheating; NO_X emissions; numerical simulation*

1. Introduction

The energy consumption in China is dominated by coal consumption, which account for 55.3% of total energy consumption in 2024. The share of total energy consumption accounted for by clean energy sources, including natural gas, hydropower, nuclear power, wind power and solar power, is 26.4% [1]. Thermal power installed capacity accounts for 47.62% of the total installed power capacity

at the end of 2023, up 4.1% year-on-year. Therefore, despite the gradual development of new energy, thermal power is still in an irreplaceable position in China's power system in the short term.

Coal-fired power plants are one of the primary sources of NO_X. [2, 3]. In 2020, China revised its emission standards for coal-fired power plants. The revised standards included the implementation of an ultra-low NO_X emission standard, with a NO_X emission limit of 50 mg/Nm^3 at 6% O_2 [4]. Currently, coal-fired power plants mainly use flue gas denitrification and low NO_X combustion technologies to attain the objective of ultra-low NO_X emissions. The process of flue gas denitrification employs two distinct reduction mechanisms: selective non-catalytic reduction (SNCR) and selective catalytic reduction (SCR) [5, 6]. Low-NO_X combustion technology adopts air-staged combustion [7, 8], fuel-staged combustion [9, 10], flue gas recirculation [11, 12], and low-NO_X burner [13, 14]. Flue gas denitrification technology has high nitrogen reduction efficiency and simple equipment, but the equipment of this technology is expensive and has high operating costs. There are a series of problems such as air preheater clogging and secondary pollution caused by waste deactivated catalysts. Low NO_X combustion technology has low initial investment and no operating cost, but the nitrogen reduction efficiency is relatively low [15]. Traditional low NO_X combustion technology is facing challenges under today's stringent NO_X emission standards. Therefore, the development of new low-NO_X combustion methods to realize the high efficiency and cleanliness of NO_X emissions is an urgent problem to be solved at present.

Pulverized coal preheat combustion technology [16] is a clean and efficient combustion technology that holds great promise in the field of NO_X reduction. Ouyang et al. [17] put forward a combustion technology founded on the self-sustained preheat combustion. They further investigated the combustion characteristics and NO_X emission of bituminous coal on a newly developed self-sustained preheat combustion test bed. The results show that pulverized coal can be cleanly and efficiently utilized by the self-sustained preheat combustion technology. The NO_X emission is reduced to 72 mg/Nm^3 (@6% O_2) and the resultant combustion efficiency is as high as 98.4%. Song et al. [18] developed a new type of pulverized coal self-sustained preheat combustion technology for ultra-low volatile fuels and set up a corresponding 16MW pilot plant. The findings indicate that the combustion efficiency consistently exceeds 96% across all cases, with the lowest NO_X emission recorded at 110 mg/m^3(@6% O_2). Hui et al. [19] examined the variable load properties and thermal modification of disparate coal types utilizing preheated combustion technology on a 40kW$_{th}$ test stand. The results show that the preheated combustion technology exhibits characteristics of adaptability with respect to coal rank and variable load. The preheating process has been shown to enhance the stability of coal combustion under low load conditions. Wang et al. [20] conducted a study to examine the impact of self-preheating technology on fuel preheating, modifications, combustion characteristics, and NO_X emissions. The findings indicates that the implementation of self-preheating technology enhances the combustion efficiency and reliability of the fuel, thereby achieving effective combustion and a substantial reduction in NO_X emissions across a considerable load spectrum. Zhu et al. [21, 22] explored the low-load characteristics of pulverized coal combustion based on the preheat combustion technology on a test platform. The ignition and combustion stability of pulverized coal at low loads are found to be greatly improved by preheated gas with high heating value and preheated coal with high physical sensible heat. The pre-denitrification during preheating helps reduce NO_X emissions. Zhu et al. [23] carried out a comparative experimental study of conventional combustion and preheated combustion on a laboratory-scale preheated combustion furnace. The results show that preheated combustion results in significant reductions in particulate

matter (PM) and NO. Ding et al. [24] discovered that the combustion performance of the preheated coal, a fuel close to the gaseous fuel, is much better than that of raw coal. Lv et al. [25] investigated the combustion characteristics and NO emission of semi-coke preheated combustion over a wide range of preheat temperatures. The results show that rising the preheating temperature can lead to a further reduction in NO emission and an enhancement in combustion efficiency. At a preheating temperature of 1400°C, NO emission can be reduced by up to 74%. The preheating combustion technology of pulverized coal has been demonstrated to enhance the ignition and combustion stability of pulverized coal, leading to a reduction in NO_X emissions. Additionally, it exhibits robust fuel adaptability, enabling operation in conditions conducive to peak shaving.

Based on pulverized coal preheating combustion technology, our team designs and develops a novel burner - SSIC burner. A series of studies have been conducted by our team to investigate the performance and potential applications of this burner. Tang et al. [26] designed a pulverized coal SSIC burner and established an experimental system for the SSIC burner. The results show that the burner is able to realize stable self-sustained combustion in different load ranges, with good anti-interference ability and fast start-stop function. Afterwards, they [15] conducted tests on a pilot pulverized coal combustion system. The objective of the tests is to investigate the effect of the SSIC burner on the combustion characteristics of the furnace. The findings indicate that the burner is capable of reliably preheating pulverized coal to temperatures in excess of 700°C. The release and subsequent combustion of pyrolysis gases has been demonstrated to enhance the combustion characteristics within the boiler, thereby reducing NO_X emissions. This improvement occurs without the necessity of implementing additional NO_X reduction equipment. Yao et al. [27] advanced a novel preheating-based peaking method and investigated the preheating effect of the SSIC burner at varying loads. The findings indicate that the burner preheating effect is substantial, yielding elevated temperatures and a considerable volume of pyrolysis gas. The NO_X emission levels are recorded at 91.53 mg/Nm^3, and the emission reduction efficiency attains 95.9%. The SSIC burner is not only small in size, simple in structure and low in retrofitting cost, but also has the advantages of stable pulverized coal preheating and remarkable NO_X reduction effect. However, extant research has primarily centered on the design optimization of the SSIC burner, while its application in industrial boilers has received comparatively less attention.

In comparison with the experimental platform, the wind-dust interaction in industrial boilers is more pronounced. Furthermore, the flow and combustion of pulverized coal is more complex. It is necessary to explore the application of the SSIC burner on the industrial boiler. Therefore, according to the findings of the team members' research, the present study investigates the combustion and pollutant production characteristics before and after the application of an SSIC burner in a 330-megawatt tangentially fired boiler. A physical model of the boiler is constructed, with the dimensions corresponding precisely to those of the original apparatus. The physical model of the boiler is built on a one-to-one basis based on actual data, and the model is modified based on the verification of the model's accuracy. The E-layer dense and light burner is replaced with a SSIC burner because the E-layer is closer to the reduction zone. The 330MW power plant boiler is often operated at 70% load, so numerical simulation studies are carried out for the boiler before and after the retrofit at 100% and 70% loads, respectively. The detailed comparative analyses of the velocity field, temperature field, component field, and NO_X generation in the furnace are carried out before and after the retrofit at different loads. The results of the numerical calculations provide a detailed reference for the application of the SSIC burner on the boiler.

2. Tangentially fired boiler

The configuration of the boiler structure and the arrangement of the burner are illustrated in Figure 1(a). The boiler's height is 54046 mm, the horizontal cross-section of the furnace is 14022 mm × 13640 mm, and the inclination angle of the ash hopper is 55°. The division panel superheater (DPSH), platen superheater (PLSH) and reheater (RH) are arranged from front to back at the top of the furnace. The burners are arranged in groups at the corners of the furnace. The furnace consists of a main combustion zone and a burnout zone. The main combustion zone has 13 layers of nozzles, 5 of which are primary air nozzles. They are designated A, B, C, D and E from bottom to top. The primary air is divided into two groups along the height direction, with the lower three layers as a group and the upper two layers as a group. The A and B layers are plasma burners with perimeter air. The C, D and E layers use lean burners, with the bottom dense and top light mode in layers C and E, and the top dense and bottom light mode in layer D. The 8 layers are secondary air nozzles, which are indicated by AA, AB, BC, CC, DD, DE, EE and FF from the bottom to the top. The primary and secondary air nozzles are evenly spaced. The boiler is arranged with four layers of SOFA, indicated from bottom to top by SOFA1, SOFA2, SOFA3 and SOFA4. P1 is shown in Figure 1(a) as a diagonal cross-section of the boiler.

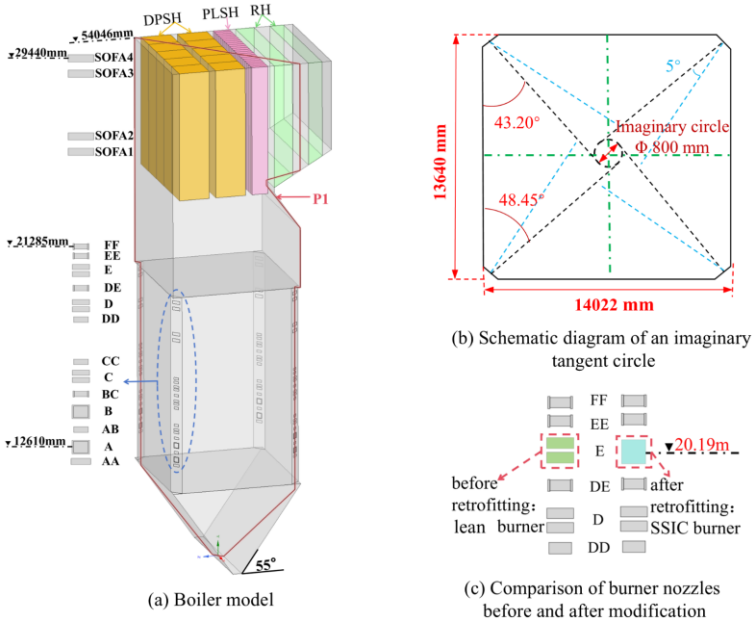

Fig. 1 Boiler structure

Figure 1(b) shows the imaginary tangent circle of the boiler cross section. The angles between the centerline of the burner outlet jet and the centerline of the water wall are 48.45° and 43.20°, respectively. Primary air and SOFA prolongation forms a virtual circle of 800 mm diameter at the furnace center, and the secondary air has a 5° angle to primary air. When the SSIC burner is applied to a 330 MW tangentially fired boiler, the boiler primary air nozzle needs to be modified: the nozzle with dense and light burner installed on the E-layer is changed to a nozzle of the same size as the outlet of the SSIC burner. Figure 1(c) shows the modified burner arrangement structure. The modified E-layer burner center elevation is 20.19m.

3. Numerical simulation

3.1. Grid system

The grid structure of the boiler is shown in Figure 2. To minimize the calculation costs while ensuring the accuracy of the calculation, the part of the boiler from the ash hopper to the boiler outlet is selected as the calculation area. The entire calculation area is divided into three parts: ash hopper, combustion zone and upper furnace. The first step is to mesh the three regions separately. To obtain more accurate simulation results, a high-quality ortho-hexahedral structured mesh is used for the whole region of the model, and the number of meshes in each region depends on the complexity of the reaction. The combustion reaction transpires predominantly within the primary combustion zone and in the vicinity of the furnace, adjacent to the burner nozzles, so the grid is structured in such a way to minimize the numerical simulation error. The grid in the furnace cross-section coincides with the direction of flow of coal particles entering the boiler from the burner as a means of reducing pseudo-diffusion due to the grid not coinciding with the direction of particle flow. Then, the meshes of the three regions are coupled and spliced by interface boundary conditions [28]. In addition, due to the complexity of the mesh structure, some simplifications have been made to the meshing. DPSH, PLSH and RH is simplified to zero-thickness walls [29].

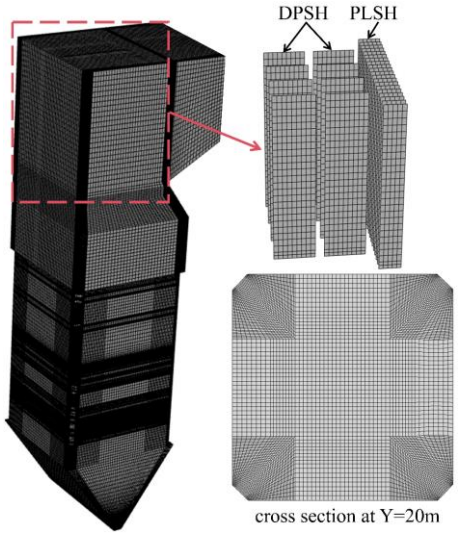

Fig. 2 Grid structure of boiler

To guarantee both the precision and expediency of numerical results, the grid of the combustion region is meshed and refined step by step. Orthogonal quality exceeds 0.7. Skewness is less than 0.3. Three grids with different number of cells are selected with the numbers of cells being 1,276,365, 1,815,440, and 2,194,047, respectively. Numerical simulations are performed with these grids to verify the grid-independence under the same operating conditions.

As illustrated in Figure 3, the numerical simulation results of the mean temperature and O_2 concentration of the horizontal cross-section along the height direction of the furnace at varying grid numbers are presented. There is a significant deviation between the computed results at grid number 1,276,365 and the computed results at grid numbers 1,825,440 and 2,194,047, whereas the calculation results of the grid model with 1,825,440 and 2,194,047 cells are closer to each other. Subsequent calculations are performed on a grid comprising 1,825,440 cells.

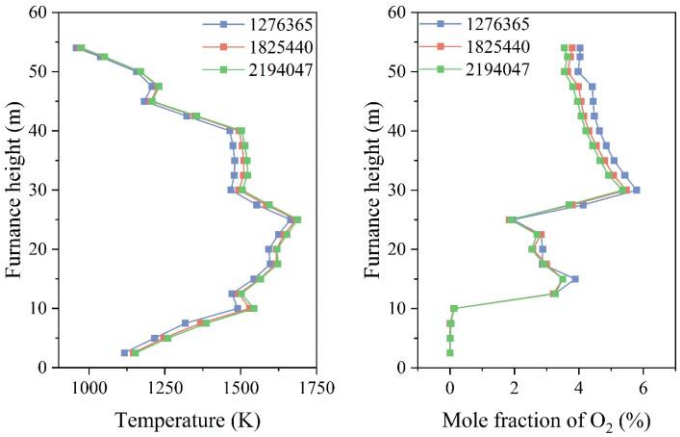

Fig. 3 Mean temperature and O_2 concentration of horizontal section

3.2. Numerical model

The numerical simulations are executed using the commercial code ANSYS FLUENT, version 2020. The thermochemical reaction of pulverized coal within a boiler system encompasses numerous complex physical processes. These processes include turbulent gas flow, particle motion, convective and radiative heat transfer, volatile analysis, coke combustion, and NO_X generation. The realizable *k-ε* model is selected to simulate the gas phase turbulent flow in the tangentially fired boiler. The utilization of this model enables a more precise description of turbulent motion and facilitates the calculation of optimal combustion process parameters within the furnace [30, 31].

The present paper employs a stochastic particle trajectory model in the Lagrange coordinate system to investigate the trajectory and combustion process of coal particles within a gas-solid two-phase flow [32, 33]. The equilibrium equations for the forces acting on the particles have the form shown in equation (1) in the coordinate system:

$$\frac{du_p}{dt} = F_D\left(u - u_p\right) + \frac{g_x\left(\rho_p - \rho\right)}{\rho_p} + F_x \tag{1}$$

Where F_x and F_D expressions are as in equations (2) and (3), respectively:

$$F_x == \frac{1}{2}\frac{\rho}{\rho_p}\frac{d}{dt}\left(u - u_p\right) \tag{2}$$

$$F_D = \frac{18\mu}{\rho_p d_p^2}\frac{C_D \,\mathrm{Re}}{24} \tag{3}$$

Where ρ_p is particle density, u_p is particle velocity.

The discrete ordinates model has been selected for the purpose of investigating the radiative heat transfer process in the furnace [34]. The model has a wide range of applicability for radiative heat transfer in semi-transparent media and non-ash bodies. The model incorporates the effects of particles and is suitable for solving combustion problems with surface radiation. The calculation of the absorption coefficients of gas-phase mixtures is performed using the weighted-sum-of-gray-gases (WSGGM) method [35], and the particle emissivity is set to 0.9 [36].

A single-step pyrolysis model is used for the de-volatilization reaction of coal [37]. The specific equation is expressed as equation (4):

$$\frac{dm}{dt} = A\exp\left(\frac{-E}{RT_p}\right)\left(m_0 - m\right) \tag{4}$$

Where m_0 is initial volatile mass, m is post-reaction volatile mass, T_p is particle temperature, R is universal gas constant.

The kinetic-diffusion controlled reaction rate model provides a satisfactory fit to the simulation of combustion on the surface of coke particles. A kinetic diffusion-controlled reaction rate model is employed to simulate combustion on the surface of coal particles [38]. As delineated in equation (5), the diffusion rate coefficient is exhibited in this model. The kinetic rate is shown in equation (6):

$$D_0 = C_1 \frac{\left[\left(T_p + T_\infty\right)/2\right]^{0.75}}{d_p} \tag{5}$$

$$R = C_2 e^{-\left(E/RT_p\right)} \tag{6}$$

The coke burning rate based on the different weighting of these two coefficients is given in equation (7):

$$\frac{dm_p}{dt} = -\pi d_p^2 p_{ox} \frac{D_0 R}{D_0 + R} \tag{7}$$

Where T_∞ is gas phase temperature, p_{ox} is partial pressure of O_2 around the particle.

A post-processing approach is utilized to simulate NO_X generation [39]. This approach is based on the flow field, temperature field, and component concentrations. NO_X is generally categorized as prompt NO_X, thermal NO_X, and fuel NO_X. The proportion of prompt NO_X within the total NO_X is minimal, accounting for less than 5%, which is often negligible. Thermal NO_X is more sensitive to changes in temperature and the Zeldovich mechanism [40] is employed to ascertain its specific formation mechanism. The reaction equations involved are shown in equations (8) to (10):

$$N_2 + O \longleftrightarrow N + NO \tag{8}$$

$$N + O_2 \longleftrightarrow O + NO \tag{9}$$

$$N + OH \longleftrightarrow H + NO \tag{10}$$

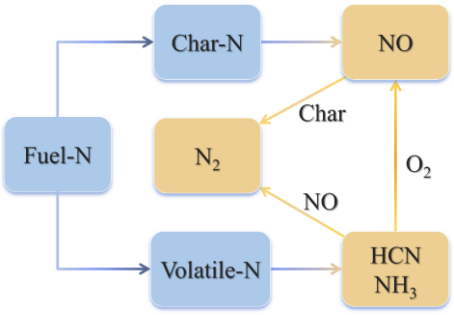

Fig. 4 Fuel NO_X generation mechanism

The formation of fuel NO_X is primarily attributable to the decomposition of nitrogen compounds present within the fuel during the combustion process, of which the proportion of NO is up to 90%. The generation of fuel NO is based on the De Soete model [41]. As illustrated in Figure 4, the specific mechanism is evident [42]. Fuel nitrogen (Fuel-N) is comprised of char nitrogen (Char-N) and volatile nitrogen (Volatile-N). Volatile-N can be oxidized to form NO via the reaction of the intermediates HCN and NH_3 with O_2 in the fuel-lean region or with NO in the fuel-rich region to form N_2. The ratio of HCN to NH_3 during the evolution of Volatile-N is 9 for bituminous coal, while coke is completely oxidized to NO, according to the Fluent user manual [43, 44].

3.3. Case setup and boundary conditions

The fuel used in the boiler is a representative Shenhua bituminous coal. The proximate and ultimate analyses are presented in Table 1. The coal powder's particle size distribution adheres to the Rosin-Rammler distribution. The diameter distribution of coal particles ranges from 5.83 to 230 with an average particle size of 62 um and a dispersion factor of 1.12. Case 1 is 100% load of the boiler before E-layer burner modification. The name is set to 100 and is an experimental validation case. Case 2 is 100% load of the boiler after E-layer burner modification, and the name is set to 100E. A comparison of the calculation results from Cases 1 and 2 facilitates the exploration of the effect of the SSIC burner on the internal combustion characteristics of the furnace.

Table 1. Proximate and ultimate analyses of Shenhua bituminous coal. (ar, as received)

	Proximate Analysis (%)				Ultimate Analysis (%)				
	M_{ar}	A_{ar}	V_{ar}	FC_{ar}	C_{ar}	H_{ar}	O_{ar}	N_{ar}	S_{ar}
Shenhua coal	14.50	7.37	27.8	50.33	64.03	3.26	9.76	0.77	0.31

Table 2. Numerical simulation cases setup.

	Title	SSIC burner	Conventional burner	Boiler load
Case1	100	-	ABCDE	100%
Case2	100E	E	ABCD	100%
Case3	70	-	BCDE	70%
Case4	70E	E	BCD	70%

Peak load operation is frequently necessary in power plants, prompting alterations in boiler load. Consequently, the quantity of incoming fuel, the volume of combustion air, the flow and the temperature field in the furnace undergo significant modifications. The ability of the boiler to adapt to variable load after the application of SSIC burner is an important parameter to examine the performance of SSIC burner. Therefore, Case 3 and 4 are set up as cases with 70% load of the boiler before and after modification, and the case names are set as 70 and 70E, respectively. By comparing the calculation results of Case 3 and 4, the changes of velocity field, temperature field, component field and NO_X generation inside the furnace before and after the application of the SSIC burner at 70% load are investigated. The input pulverized coal mass flow is kept constant for the same load and the specifics of the case setup are shown in Table 2. The inlet parameters of the boiler at 100% and 70% loads are shown in Table 3.

Table 3. Boiler inlet parameters.

	100% load		70% load	
	Mass flow (kg/s)	Temperature (K)	Mass flow (kg/s)	Temperature (K)
Primary air	112.75	343	84.48	343
Secondary air	126.41	614	94.72	614
SOFA	102.50	614	76.80	614
Total coal	33.33	343	25.01	343

The inlet boundary for the calculation is the burner nozzle cross section located around the combustion zone of the furnace. The mass flow rate is used in the inlet boundary condition. The gas-phase velocity and the coal particle flow rate on the gas-phase boundary are calculated according to specific operating conditions. The SSIC burner output conditions serve as boiler input conditions, with data obtained from field testing. Specific parameters are detailed in Reference [32]. Assuming that the inlet velocity of coal particles is 0.9 times of the primary airflow. The collision of pulverized coal with the wall is an elastic collision. The

pulverized coal temperature is equal to the temperature of the primary airflow. Assuming that the cross-sectional flow is a fully developed flow and ignoring the gradient of the dependent variable in the direction of flow. The furnace outlet has been designated as a pressure outlet boundary condition, with an outlet pressure set to -80 Pa. The standard wall function is used to simulate the wall effects for the boiler water wall region. The wall is used for convective heat transfer. The heat transfer coefficient is thus established at 410W/(m^2·K) and the wall radiation factor is taken as 0.6. The operating temperatures of DPSH, PLSH and RH are set to constant temperatures of 736 K, 766 K and 794 K, correspondingly.

3.4. Model validation

The simulated boundary conditions closely resemble the experimental conditions. A comparison of the calculated and experimental results is given in Table 4. The deviations of the O_2 concentration, temperature, and NO concentration at the furnace outlet do not exceed 3.2%, 3.1%, and 2.6%, respectively. These values are all found to be less than the acceptable limits for industrial calculations. It has been determined that the established boiler model is capable of accurately simulating its actual operational characteristics.

Table 4. Experimental validation of numerical simulation.

	Simulation results	Experimental results	Errors (%)
O_2 content (%)	3.83	3.71	3.13
Temperature (K)	1128	1163	3.10
NO_X emission (mg/Nm^3)	184.42	189.18	2.58

4. Results and discussion

4.1. Velocity distribution

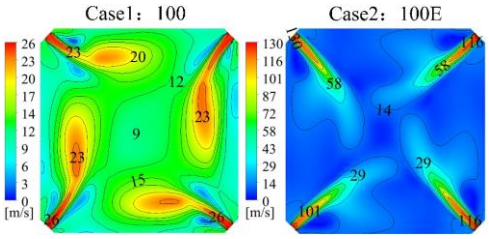

(a) Velocity distribution in the E-layer at 100% loading (Y=20m)

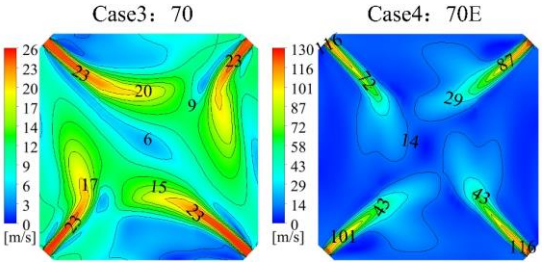

(b) Velocity distribution in the E-layer at 70% loading (Y=20m)

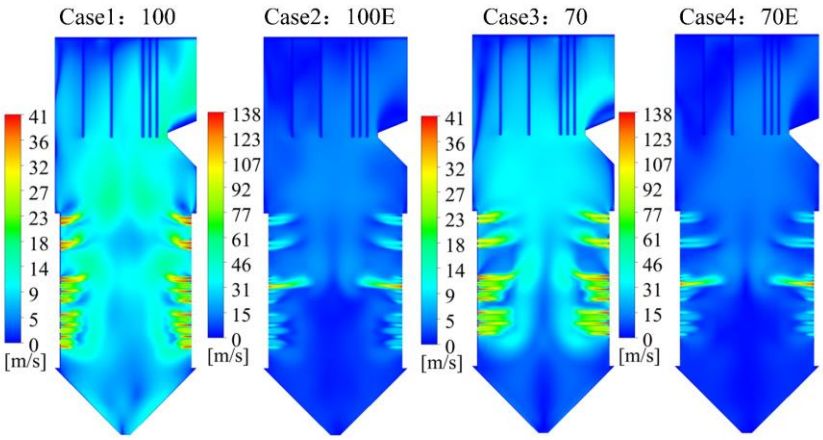

(c) Velocity distribution of P1 section under different loads

Fig. 5 Velocity distribution in the furnace

Figure 5 shows the velocity distribution contours of E-layer burner cross-section and P1 cross-section before and after boiler modification at 100% and 70% loads. The gas stream from the burner nozzle forms a more pronounced tangent circle in the center of the furnace at 100% load, as illustrated in Figure 5(a). After the modification, the velocity at the primary air nozzle of the E-layer increases significantly. The mean velocity of the E-layer cross-section increases from 13.45 m/s to 19.10 m/s with an increase of 5.65 m/s. The rigidity of the airflow is strengthened. Pulverized coal releases some of its heat after preheating in a SSIC burner, generating high-temperature pyrolysis gas and coke. The energy transfer from the combustion reaction inside the self-sustaining internal combustor results in high kinetic energy and increased rigidity of the gas-solid mixture. The velocity of the E-layer is increased after the modification, and this phenomenon facilitates stable combustion in the boiler.

As demonstrated in Figure 5(b), the airflow near the burner is more active compared to that of other locations, with lower velocities near the core and near-wall region of the furnace. At the four corners of the boiler, the primary and secondary air interact with each other, thereby forming a clockwise rotating airflow in the center of the furnace. This phenomenon is similar to the change in the velocity field before and after the boiler modification at 100% load. The average velocity of the modified E layer increased from 10.26 m/s to 17.52 m/s with an increase of 7.26 m/s, which is higher than the lift at 100% load. However, given the reduction in the total coal and air volume necessary for boiler operation due to the load reduction, the average airflow velocity of the E- layer cross-section before and after the modification is both slightly reduced at 70% load.

As illustrated in Figure 5(c), the velocity distribution contours of P1 cross-section exhibit significant alterations following boiler modification under varying load conditions, namely 100% and 70%, respectively. Figure 5(c) shows the velocity distribution contours of P1 cross-section before and after boiler modification from 100% and 70% loads. Air from the main combustion zone and the burnout zone of the primary air, secondary air, and SOFA air nozzle injection into the furnace. The coal particles and air mixing in the furnace to form a tangent circle combustion. Consequently, the main combustion zone and the burnout zone of the air velocity are larger, and the bottom of the cold ash hopper and the tail of the furnace air velocity are small. In addition, the velocity at the primary air nozzle of the modified E-layer is higher than that at the nozzles of the other layers under both loads.

4.2. Temperature distribution

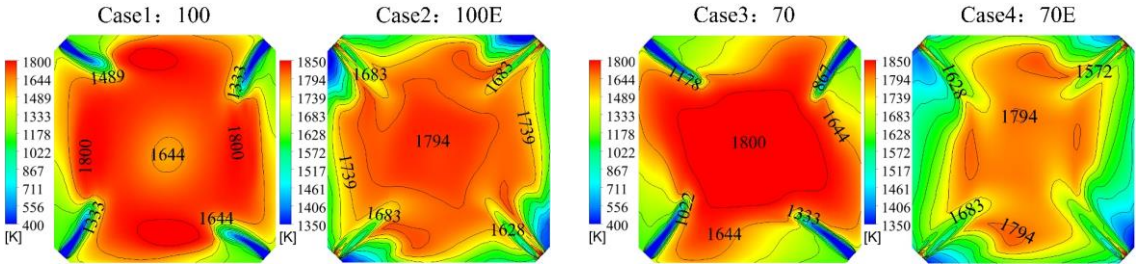

(a) Temperature distribution in the E-layer at 100% loading (Y=20m)

(b) Temperature distribution in the E-layer at 70% load (Y=20m)

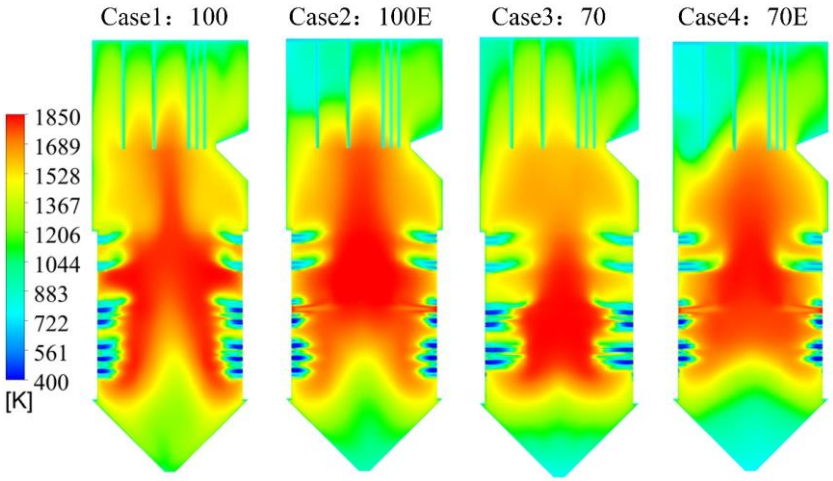

(c) Temperature distribution of P1 section under different loads

Fig. 6 Temperature distribution in the furnace

Figures 6 (a) and (b) demonstrate the temperature distribution contours in the E layer cross-section of the boiler before and after the application of the SSIC burner at 100% and 70% loads, respectively. The average temperatures of the modified E-layer cross-section under both 100% and 70% loads change significantly from 1613 K and 1611 K to 1728 K and 1688 K. Pulverized coal undergoes preheating in the SSIC burner, so the temperature of the gas stream at the entrance of the furnace is higher. Meanwhile, the pulverized coal fires prematurely, leading to the enlargement of the hypothetical tangent circle of the modified boiler. The pulverized coal burns more fully after preheating, thus increasing the mean temperature of the cross-section. In addition, the 75% load makes a longer ignition distance, a smaller diameter of the hypothetical tangent circle, and a reduction in the localized high temperature zone compared to 100% load.

Figure 6(c) demonstrates the temperature distribution of the P1 cross section before and after the boiler modification at 100% and 70% load. The temperature distribution within the furnace is found to be uniform both before and after the boiler modification, and the distribution remains almost the same. The combustion is the most intense in the burner area, and the fastest temperature increase, which indicates that the pulverized coal spray into the furnace to achieve rapid precipitation of volatile and fire. As the flue gas rises, the temperature distribution also shows that the first two sides are high and the center is low, and then the center is high and the two sides are low. The overall temperature of the cross-section increases after the modification, especially in the area near and above the E-layer burner, and the overall flame center shifts upward. The reduction in load at 70% load leads to a reduction in localized high temperature areas compared to 100% load.

4.3. Components distribution

Figures 7 (a) and (b) show the average O_2 mole fraction distribution in the cross-section of the E-layer burner prior to and following the boiler modification at 100% and 75% loads, respectively. The O_2 mole fraction of the modified E-layer cross section decreases significantly. O_2 is consumed by the combustible gases in the SSIC burner, which results in oxygen-poor conditions in the furnace. A reducing atmosphere is formed, which in turn inhibits NO_X generation. Figure 7(c) shows the contours of O_2 mole fraction distribution in the P1 section before and after the modification at different loads of the boiler. The O_2 distribution of the P1 cross-section did not change much before and after the modification, which is due to the fact that the ratio of total coal to total air input remains basically the same, and the elemental carbon is conserved. Furthermore, an analysis of Figure 7(c) and Figure 6(c) shows an opposite trend in the distribution of O_2 and temperature on the main combustion zone.

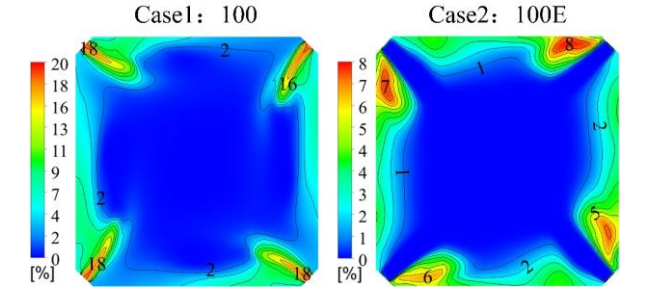

(a) O_2 distribution in E-layer at 100% loading (Y=20m)

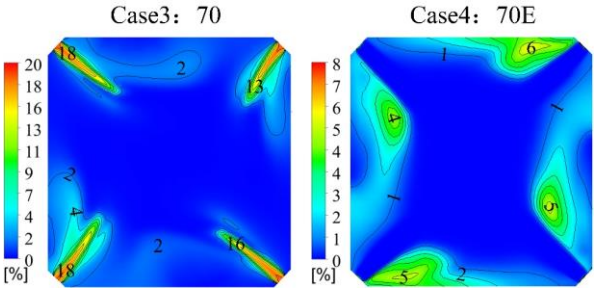

(b) O_2 distribution in E-layer at 70% loading (Y=20m)

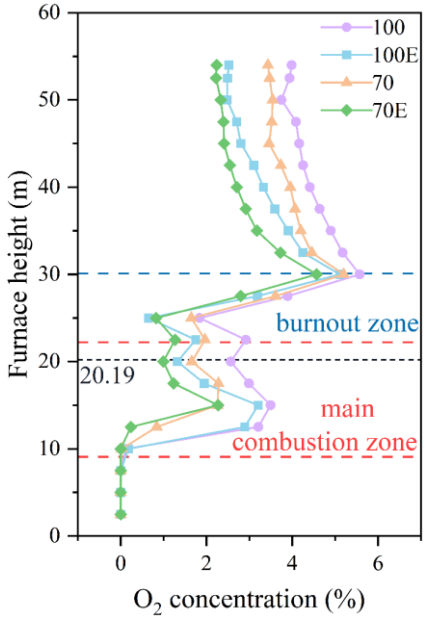

(d) Cross-sectional average O_2 concentration

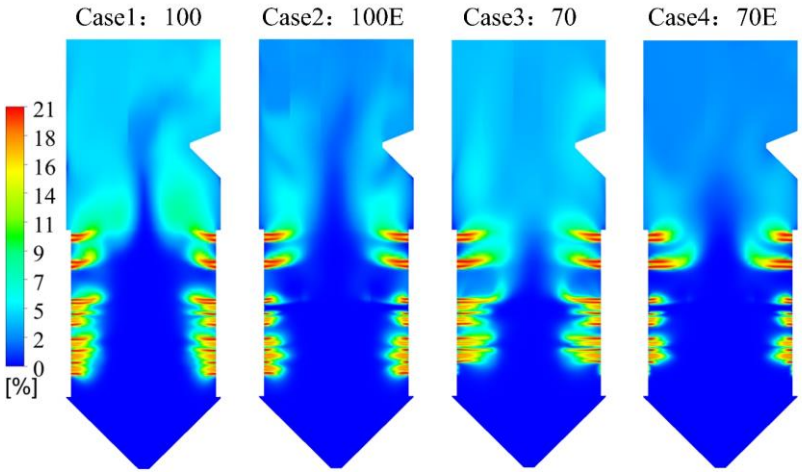

(c) O_2 distribution under different loads

Fig. 7 O_2 distribution in the furnace

Figure 7(d) shows the distribution pattern of cross-sectionally averaged O_2 concentration along the boiler's height direction for varying operating conditions. A comparison of Case 1 and Case 2, as well as Case 3 and Case 4, respectively, indicates that the trend of the boiler before and after the modification is essentially

analogous under both 100% and 70% load operating conditions. In the main combustion zone, a substantial quantity of air from the burner into the furnace, causing the O_2 concentration to begin to rise, and the fluctuations in the O_2 concentration are more pronounced. In the main combustion zone, pulverized coal is carried and sprayed into the furnace by the primary air. The volatile present in pulverized coal is rapidly precipitated and mixed with the secondary air to burn. This process consumes a substantial amount of O_2, thereby reducing the overall O_2 concentration in the main combustion zone. Meanwhile, due to the arrangement of the boiler's secondary air and primary air in close proximity to each other, resulting in the simultaneous supplementation and depletion of O_2. Volatiles are basically burned off with the increase of the furnace height, and a substantial quantity of SOFA air is added, resulting in a significant increase in O_2 concentration. After that, the incomplete burned coke further fires and burns out, and the O_2 concentration gradually decreases to a stable value.

Figure 8(a) demonstrates the distribution of the CO mole fraction in the cross-section of the E-layer burner before and after the modification at 100% load of the boiler. The cross-sectional average CO mole fraction of the modified E layer increases from 0.16% to 0.42%. The pulverized coal undergoes volatile pyrolysis and coke gasification to generate a large amount of CO in the SSIC burner, which is subsequently fed into the furnace for combustion. Pre-pyrolysis combustion in the SSIC burner is equivalent to in-depth air classification. The pulverized coal is pre-treated in the SSIC burner to allow longer time and more sufficient space for volatile pyrolysis and coke gasification to promote the internal reduction reaction.

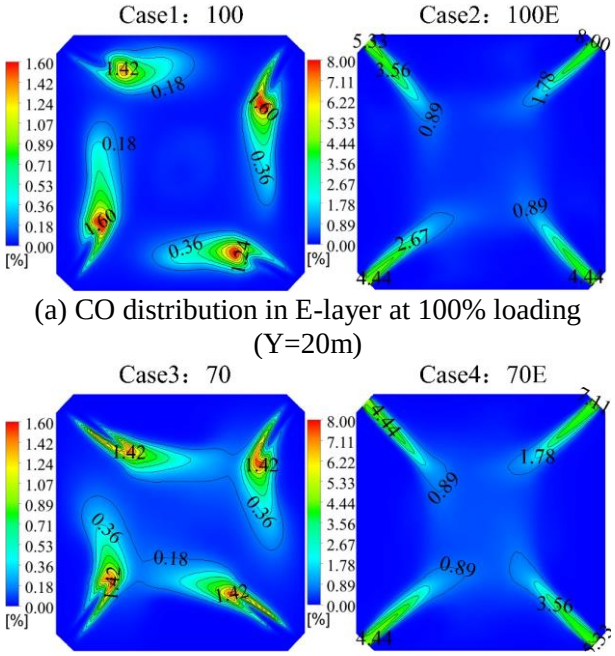

(a) CO distribution in E-layer at 100% loading (Y=20m)

(b) CO distribution in E-layer at 70% loading (Y=20m)

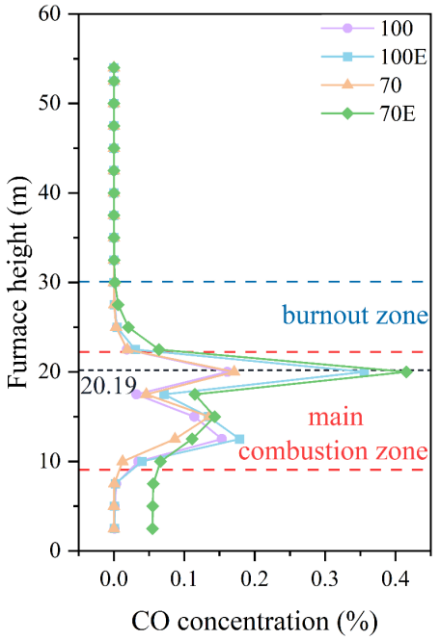

(c) Cross-sectional average CO concentration

Fig. 8 CO distribution in the boiler

Figure 8(b) demonstrates the distribution of CO mole fraction in the E layer cross-section before and after the 70% load. CO generated by pulverized coal in the SSIC burner is introduced into the furnace from the burner outlet, resulting in a substantial increase in the CO concentration in the primary air cross section of the E-layer where the SSIC burner is installed. The average CO mole fraction increases from 0.16% to 0.47%.

Figure 8(c) demonstrates the distribution pattern of average CO concentration along the cross-section in the direction of the height, from which the trend of CO concentration under each condition is basically the same. The main combustion zone is characterized by an oxygen deficiency, resulting in incomplete

combustion of the pulverized coal, leading to the generation of CO. As the airflow rises, combustion in the burnout zone, where there is sufficient air volume, gradually reacts completely. The generated carbon monoxide is thoroughly oxidized to carbon dioxide, leading to a gradual decline in the CO concentration along the height. In addition, the CO concentration in the furnace increases after the retrofit, especially near the center elevation of the SSIC burner at 20.19m, where the CO concentration increases sharply.

Figure 9 demonstrates the CO_2 distribution in the furnace before and after the modification at 100% and 70% loads. The CO_2 mole fraction before and after the transformation basically remains unchanged. The distribution contours of CO_2 and O_2 mole fraction basically corresponds to each other, and the distribution of the two is opposite. This is because CO_2 is mainly generated by the combustion reaction between CO and O_2. The part with high CO concentration has low O_2 concentration. There is little difference in the CO_2 mole fraction in the E-layer cross section prior to and following the boiler modification. The total amount of input pulverized coal remains constant, thereby ensuring that the total mass of elemental carbon remains constant as well. The final CO_2 concentration is basically the same even though the concentration of the intermediate product CO varies considerably after the modification.

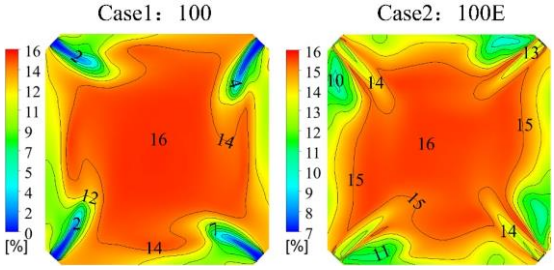

(a) CO_2 distribution in the E-layer at 100% loading (Y=20m)

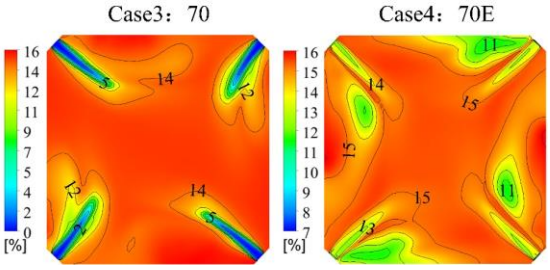

(b) CO_2 distribution in the E-layer at 70% loading (Y=20m)

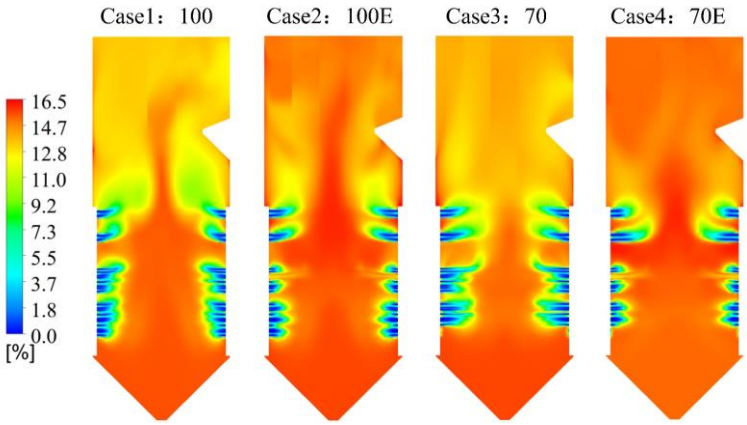

(c) Distribution of CO_2 under different loads

Fig. 9 CO_2 distribution in the boiler furnace

Figure 10(a) demonstrates the NO_X concentration in the cross-section of the E-layer burner prior to and following the boiler modification at 100% load. The average NO_X concentration in the cross-section of the E-layer burner is reduced from 178.67 mg/Nm^3 to 127.89 mg/Nm^3 after the modification, which is a reduction of 50.78 mg/Nm^3, but there are still a few small areas with high NO_X concentrations. During the process of pulverized coal combustion, the generation and reduction of NO_X occur via two distinct pathways. The pathways of NO_X generation can be categorized into fuel NO_X, thermal NO_X, and prompt NO_X. The reduction of NO_X can be categorized into homogeneous (reducing gas) reduction and heterogeneous (coke) reduction. In the case of internal reduction, homogeneous reduction is the predominant process. Preheating of the pulverized coal in the SSIC burner is done with the primary goal of promoting the production of reducing gas. Reducing gases such as methane, H_2, and CO are produced after preheating and decomposing

pulverized coal in the SSIC burner. Hydrocarbon pyrolysis generates CH_i free radicals at high temperature, which combine with NO to form a nitrogen-containing intermediate product HCN [45]. Several regions with high NO_X concentration have high O_2 concentration, which is equivalent to an oxygen-rich and fuel-poor zone. The presence of Volatile-N in these regions facilitates the oxidation of NO through a reaction involving the intermediate products HCN and NH_3 with O_2. This process leads to the accumulation of NO_X concentrations.

Figure 10(b) demonstrates the NO_X concentration distribution in the cross-section of the E-layer burner prior to and following the boiler modification at 70% load. The mean NO concentration in the cross-section of the modified E-layer burner is decreased from 153.56 mg/Nm^3 to 114.57 mg/Nm^3, a reduction of 38.99 mg/Nm^3. Although the low NO_X region of the retrofitted E-layer cross-section is slightly reduced at 70% load compared to 100% load, the SSIC burner still played a role in reducing NO_X generation.

Figure 10(c) demonstrates the NO_X mole fraction distribution of P1 cross-section before and after boiler modification at 100% and 70% loads. The NO_X concentrations in the horizontal cross-section of the boiler are all substantially reduced, and the lowest NO_X concentrations in the P1 cross-section occurred near the E-layer burner where a SSIC burner is applied. Under fuel-rich conditions, the intermediate products HCN and NH_3 react with NO to form N_2. Consequently, the average NO_X concentration in the E-layer cross-section where the SSIC burner is applied is drastically reduced.

Figure 10(d) shows the distribution pattern of cross-sectional mean NO_X concentration along the boiler height direction for 100% and 70% loads. The changes in the cross-sectional average NO_X production curves before and after the retrofit at 100% and 70% loads are essentially the same. In the main combustion zone, pulverized coal is injected into the furnace along with the primary air, which generates NO_X due to the high temperature. Meanwhile, the pulverized coal consumes O_2 for combustion, which generates part of CO and forms a reducing atmosphere, making part of NO_X reduced. Consequently, there is significant fluctuation in the NO_X in the primary combustion zone. The decrease in NO_X concentration at the nozzle's height within the burnout zone is caused by the dilution of NO_X concentration due to the injection of SOFA air. The temperature rises as the coke burns out. Char-N is further oxidized to NO_X, so the NO_X concentration gradually increases again until the coke is burned out. Subsequent to modification, a reduction in the overall NO_X concentration in the furnace chamber was observed, though to varying degrees.

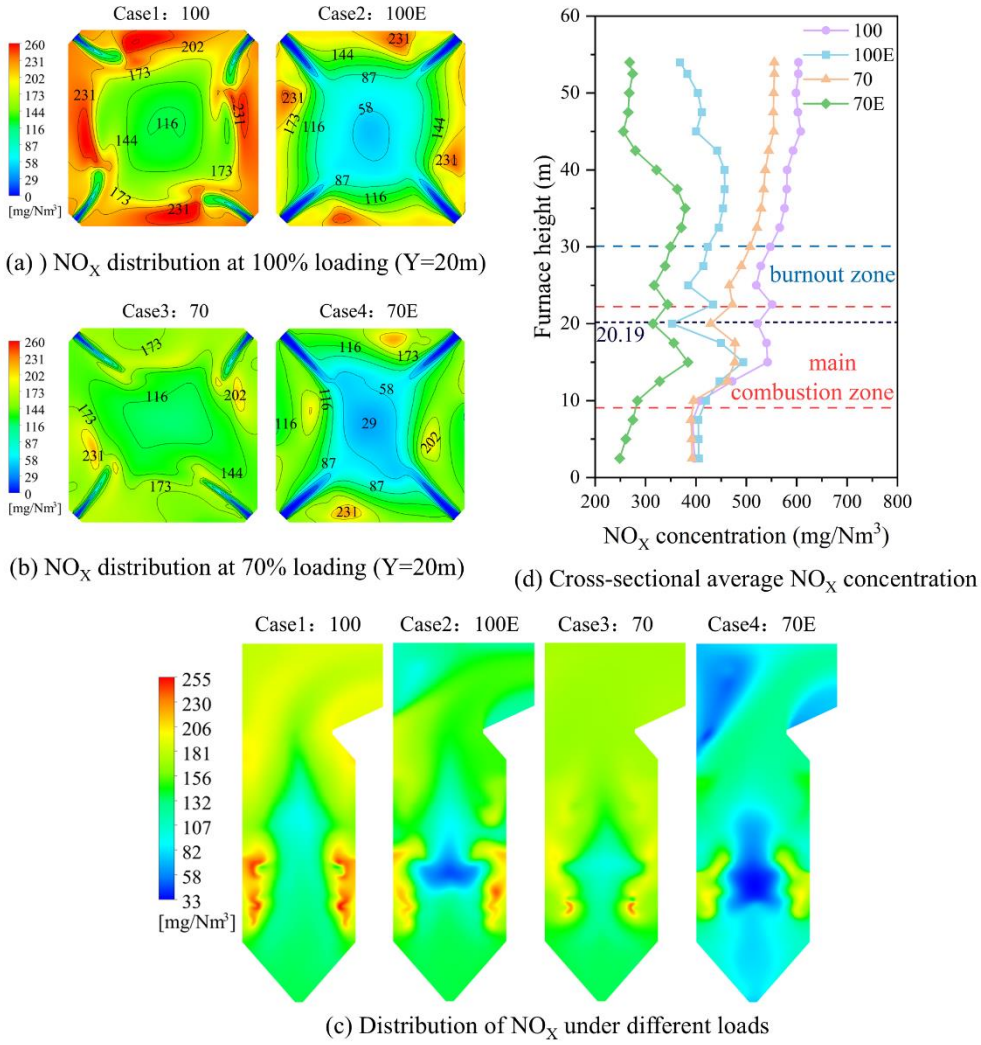

Fig. 10 NO_X distribution in the furnace

4.4. Furnace outlet parameters

Table 5 shows the NO_X concentration, O_2 and pulverized coal burnout rate at the furnace outlet before and after the application of the SSIC burner to the boiler at 100% and 70% loads. The initial NO_X emission concentration at the exit of the modified boiler is decreased by 24.77% compared with that before the modification at 100% load. The O_2 concentration and pulverized coal burnout rate are 2.40% and 98.72%, respectively. At 70% load, the initial NO_X emission concentration at the boiler outlet after the retrofit is decreased by 47.18% compared with that before the retrofit with a significant nitrogen reduction effect. Furnace outlet O_2 concentration and pulverized coal burnout rate are 2.15% and 98.35% respectively after the retrofit. Following the retrofit, the pulverized coal burnout rate increased by 2.19% and 2.42% at 100% and 70% load, respectively. This reduction in solid unburned heat loss has enhanced the plant's economic efficiency.

Table 5. Furnace outlet parameters

	100	100E	70	70E
NO_X concentration (mg/Nm^3)	184.42	138.73	173.66	91.73
O_2 concentration (%)	3.83	2.40	3.43	2.15
Pulverized coal burnout rate (%)	96.53	98.72	95.93	98.35

5. Conclusions

This study utilizes numerical simulation to investigate the applicability of the SSIC burner under varying boiler loads. The simulation is employed to explore the combustion and NO_X generation characteristics of a 330 MW tangentially fired boiler operating at 100% and 70% loads, prior to and following the retrofit of the SSIC burner. The primary conclusions that emerge from this analysis are as follows:

(1) The kinetic energy of the gas-solid mixture entering the furnace is enhanced after the application of SSIC burner. The average velocity of the cross-section of the furnace increases, and at the same time the overall stability of the air flow, which further promotes the reliable combustion in the boiler furnace. The preheated pulverized coal burns more fully in the furnace, leading to an increase in the average temperature of the furnace cross-section.

(2) The generation of combustible gases such as CH_4, H_2 and CO after the preheating of pulverized coal in the SSIC burner promotes the combustion reaction in the furnace. The CO concentration in the cross-section of the furnace rises and the O_2 concentration decreases. In addition, gases such as CH_4, CO and H_2 have reducing properties, which effectively reduces NO_X, resulting in a lower NO_X concentration in the furnace.

(3) The initial NO_X emission at the exit of the boiler with a SSIC burner is reduced from 184.42 mg/Nm^3 to 138.73 mg/Nm^3 at 100% load, and the pulverized coal burnout rate is 98.72%. At a load of 70%, the initial NO_X emission at the boiler outlet after the application of the SSIC burner is reduced from 173.66 mg/Nm^3 to 91.73 mg/Nm^3, and the pulverized coal burnout rate is 98.35%. The NO_X emission of the boiler is reduced while the burnout rate is enhanced after the application of the SSIC burner. The SSIC burner can be adapted to the variable-load operation of the 330MW tangentially fired boiler, with consideration for economic and environmental concerns.

Acknowledgment

The authors gratefully acknowledge the financial support of the National Natural Science Foundation of China (Grant No. 52376096). Dr. Tomanović appreciates support by the Ministry of Science, Technological Development and Innovation of the Republic of Serbia (Contract Annex: 451-03-136/2025-03/200017).

Nomenclature

Alphabetical Symbols	
C_D	drag coefficient /
d_p	diameter of pulverized coal particles (mm)
$F_D(u\text{-}u_p)$	drag force per unit particle mass (N)
F_x	attached mass force (N)
m	post-reaction volatile mass (kg)
m_0	initial volatile mass (kg)
p_{ox}	partial pressure of oxygen around the particle (Pa)
R	universal gas constant (8.3144 J/(kmol·K))
T_p	particle temperature (K)
T_∞	gas phase temperature (K)
u	gas phase velocity (m/s)
u_p	particle velocity (m/s)
M_{ar}	moisture, as received
A_{ar}	ash, as received

V_{ar}	volatile, as received
FC_{ar}	fixed carbon, as received
Greek Symbols	
ρ_p	particle density (kg/m^3)
u_p	particle viscosity (m^2/s)
Abbreviations	
Char-N	char nitrogen
DPSH	division panel superheater
Fuel-N	fuel nitrogen
NO_X	nitrogen oxides
PM	Particulate Matter
PLSH	platen superheater
RH	reheater
SCR	selective catalytic reduction
SNCR	selective non-catalytic reduction
SSIC	self-sustaining internal combustion
Volatile-N	volatile nitrogen
WSGGM	weighted-sum-of-gray-gases

References

[1] Wang W, Wen F, Yang Y, Jia Y. Study of the Impact of the Rise and Fall of the Coal Industry on the Regional Economy. Journal of Global Information Management. 2022;30(6):1-17.

[2] Hart J, Bhuiyan AA, Naser J. Aerodynamics of burner jet in a tangentially-fired boiler: A CFD modelling and experiment. International Journal of Thermal Sciences. 2018;129:238-253.

[3] Wang Z, Zhou H, Peng X, Cao S, Tang Z, Li K, et al. A predictive model with time-varying delays employing channel equalization convolutional neural network for NOx emissions in flexible power generation. Energy. 2024;306:132495.

[4] Qiao Y, Li S, Jing X, Chen Z, Fan S, Li Z. Combustion and NO formation characteristics from a 330 MWe retrofitted anthracite-fired utility boiler with swirl burner under deeply-staged-combustion. Energy. 2022;258.

[5] Jeon M, Lee E, Kim M, Jegal H, Park S, Chi JH, et al. Nitric oxide (NO) and nitrous oxide (N2O) emissions during selective non-catalytic reduction and selective catalytic reduction processes in a pulverized coal/Ammonia Co-fired boiler. Journal of Environmental Chemical Engineering. 2023;11(2):109398.

[6] Modliński N. Numerical simulation of SNCR (selective non-catalytic reduction) process in coal fired grate boiler. Energy. 2015;92:67-76.

[7] Jiang Y, Lee B-H, Oh D-H, Jeon C-H. Influence of various air-staging on combustion and NOX emission characteristics in a tangentially fired boiler under the 50% load condition. Energy. 2022;244:123167.

[8] Li X, Zeng L, Zhang N, Chen Z, Li Z, Qin Y. Effects of the air-staging degree on performances of a supercritical down-fired boiler at low loads: Air/particle flow, combustion, water wall temperature, energy conversion and NOx emissions. Fuel. 2022;308:121896.

[9] Shen J, Liu J, Deng S, Wang S, Chen B, Jiang X. Detailed in-furnace measurements with reburning of superfine pulverized coal in high CO2 concentration. Journal of Environmental Sciences. 2021;104:326-34.

[10] Li Y, Feng D, Sun S, Zhao Y, Shang Q, Chen K, et al. Biomass-coal reburning: Competitive mechanism of gas-solid product activation coal char. Energy. 2022;261:125225.

[11] Cheng J, Liu B, Zhu T. Experimental investigation of NOx reduction by varying internal flue gas recirculation structures in non-premixed methane combustion. Thermal Science and Engineering Progress. 2024;55:102973.
[12] Pan D, Zhu T, Ji C, Ke E. Effects of flue gas recirculation on self-excited combustion instability and NOx emission of a premixed flame. Thermal Science and Engineering Progress. 2022;30:101252.
[13] Su K, Ouyang Z, Wang H, Zhang J, Ding H, Wang W. Research on purification, combustion and NOx emission characteristics of pulverized coal preheated by a novel self-sustained purifying burner. Fuel. 2024;366:131436.
[14] Zhang H, Lin H, Zhou X, Wang X, Zheng H, Liu Y, et al. CFD modeling and industry application of a self-preheating pulverized coal burner of high coal concentration and enhanced combustion stability under ultra-low load. Applied Thermal Engineering. 2024;253:123831.
[15] Hong T, Zuodong L, Xiaoju H, Xueqiang S, Yuqiu L, Siyuan W, et al. Experimental study on combustion characteristics of a 40 MW pulverized coal boiler based on a new low NOx burner with preheating function. Energy. 2024;305.
[16] Su K, Ding H, Ouyang Z, Zhang J, Zhu S. Experimental study on effects of multistage reactant and air jet velocities on self-preheating characteristics and NO emission of burning pulverized coal. Fuel. 2022;325.
[17] Ouyang Z, Song W, Liu J, Zhu J, Man C, Zhu S, et al. Experimental study on NOx emissions of pulverized coal combustion preheated by a 2 MW novel self-sustained preheating combustor. Fuel. 2021;294:120538.
[18] Song W, Ouyang Z, Wang M, Li S, Liu J, Yu Q, et al. The combustion and NOx emission characteristics of the ultra-low volatile fuel using the novel pulverized coal self-sustained preheating combustion technology. Fuel. 2020;271.
[19] Hui J, Zhu S, Li Z, Lin J, Cao X, Lyu Q. Experimental study on peak shaving during preheating combustion for different coal ranks: Thermal modification and variable load operation. Fuel. 2024;373.
[20] Wang H, Ouyang Z, Ding H, Su K, Zhang J, Hu Y. Experimental study on the flexible peak shaving with pulverized coal self-preheating technology under load variability. Energy. 2024;289.
[21] Zhu S, Hui J, Lyu Q, Ouyang Z, Liu J, Zhu J, et al. Experimental study on pulverized coal combustion preheated by a circulating fluidized bed: Preheating characteristics for peak shaving. Fuel. 2022;324.
[22] Zhu S, Hui J, Lyu Q, Ouyang Z, Zeng X, Zhu J, et al. Experimental study on pulverized coal swirl-opposed combustion preheated by a circulating fluidized bed. Part A. Wide-load operation and low-NOx emission characteristics. Energy. 2023;284.
[23] Zhu G, Xu L, Wang S, Niu F, Li T, Hui Se, et al. Synergistic reduction on PM and NO source emissions during preheating-combustion of pulverized coal. Fuel. 2024;361.
[24] Ding H, Ouyang Z, Su K, Wang W, Zhang J, Wang H, et al. Experimental research on effects of multi-layer injection of the high-temperature preheated pulverized coal on combustion characteristics and NO emission. Fuel. 2023;347.
[25] Lv Z, Xiong X, Yu S, Tan H, Xiang B, Huang J, et al. Experimental investigation on NO emission of semi-coke under high temperature preheating combustion technology. Fuel. 2021;283.
[26] Tang H, Xu Z, Han X, Sun L, Liu Y, Shen X, et al. Design method and experimental study on a novel self-sustaining internal combustion burner. Energy. 2024;308.
[27] Yao G, Han X, Tang H, Qu J. Numerical and Experimental Study on Preheating Burner

Characteristics for Peak Shaving. Processes. 2024;12(2).
[28] Zhong Y-X, Wang X, Xu G, Ning X, Zhou L, Tang W, et al. Investigation on slagging and high-temperature corrosion prevention and control of a 1000 MW ultra supercritical double tangentially fired boiler. Energy. 2023;275.
[29] Chen S, He B, He D, Cao Y, Ding G, Liu X, et al. Numerical investigations on different tangential arrangements of burners for a 600 MW utility boiler. Energy. 2017;122:287-300.
[30] Wu X, Liu N, Lu Y, Chen Z, Li Z. Numerical Simulation of the OFA Effect on Combustion in a 600 MWe Boiler with Centrally Fuel Rich Burners. Combustion Science and Technology 2024:1-19.
[31] Tang X, Zhao C, Xing J, Cai R, Luo K, Fan J, et al. Flamelet LES of pulverized coal combustion and NO formation characteristics in a supercritical CO2 boiler. Applications in Energy and Combustion Science 2024;19:100274.
[32] Tang H, Yao G, Wang Z, Yang J, Han X, Sun L, et al. Study on low-load combustion characteristics of a 600 MW power plant boiler with self-sustaining internal combustion burners. Applied Thermal Engineering. 2025;267:125859.
[33] Yao G, Liu Z, Tang H, Meng L. Prediction of reduction products in the preheating process. Thermal Science 2023;27(5 Part B):4021-4034.
[34] Yao G, Han X, Tang H, Sun L, Liu G. Investigation of the gas-solid and Fuel-N conversion characteristics during pulverized coal preheating with an improved char model. Case Studies in Thermal Engineering. 2025;65.
[35] Yin C. Refined Weighted Sum of Gray Gases Model for Air-Fuel Combustion and Its Impacts. Energy & Fuels. 2013;27(10):6287-94.
[36] Jin W, Si F, Cao Y, Ma H, Wang Yo. Numerical optimization of separated overfire air distribution for air staged combustion in a 1000 MW coal-fired boiler considering the corrosion hazard to water walls. Fuel. 2022;309.
[37] Ma L, Fang Q, Yin C, Wang H, Zhang C, Chen G. A novel corner-fired boiler system of improved efficiency and coal flexibility and reduced NOx emissions. Applied Energy. 2019;238:453-65.
[38] Baum MM, Street PJ. Predicting the Combustion Behaviour of Coal Particles. Combustion Science and Technology. 1971;3(5):231-43.
[39] Li S, Chen Z, He E, Jiang B, Li Z, Wang Q. Combustion characteristics and NO formation of a retrofitted low-volatile coal-fired 330 MW utility boiler under various loads with deep-air-staging. Applied Thermal Engineering. 2017;110:223-33.
[40] Zeldovich YB, Sunyaev RA. 25. The Oxidation of Nitrogen in Combustion and Explosions. Conference 25. The Oxidation of Nitrogen in Combustion and Explosions.
[41] De Soete GG. Overall reaction rates of NO and N2 formation from fuel nitrogen. Symposium (International) on Combustion. 1975;15(1):1093-102.
[42] Jiang Y, Lee B-H, Oh D-H, Jeon C-H. Optimization of operating conditions to achieve combustion stability and reduce NOx emission at half-load for a 550-MW tangentially fired pulverized coal boiler. Fuel. 2021;306.
[43] Zhao S, Fang Q, Yin C, Wei T, Wang H, Zhang C, et al. New Fuel Air Control Strategy for Reducing NOx Emissions from Corner-Fired Utility Boilers at Medium–Low Loads. Energy & Fuels. 2017;31(7):6689-99.
[44] Du Y, Wang Ca, Lv Q, Li D, Liu H, Che D. CFD investigation on combustion and NO emission characteristics in a 600 MW wall-fired boiler under high temperature and strong reducing atmosphere.

Applied Thermal Engineering. 2017;126:407-18.
[45] Zhang X, Zhu S, Zhu J, Hui J, Liu Y, Zhang J, et al. Preheated combustion characteristics and fuel-nitrogen conversion paths for bituminous coal and anthracite in wide-range preheating temperature. Journal of the Energy Institute. 2023;108:101222.

Paper submitted: 21 July 2025
Paper revised: 04 September 2025
Paper accepted: 09 September 2025